

Inclusive production of heavy quarkonium η_Q via Z boson decays within the framework of nonrelativistic QCD

Xu-Chang Zheng^{1,*}, Chao-Hsi Chang,^{2,3,4,†} Xing-Gang Wu^{1,5,‡}, Xu-Dong Huang,^{1,§} and Guang-Yu Wang^{1,||}

¹*Department of Physics, Chongqing University, Chongqing 401331, People's Republic of China*

²*Key Laboratory of Theoretical Physics, Institute of Theoretical Physics, Chinese Academy of Sciences, Beijing 100190, People's Republic of China*

³*School of Physical Sciences, University of Chinese Academy of Sciences, Beijing 100049, People's Republic of China*

⁴*CCAST (World Laboratory), Beijing 100190, People's Republic of China*

⁵*Chongqing Key Laboratory for Strongly Coupled Physics, Chongqing 401331, People's Republic of China*

 (Received 9 April 2021; accepted 28 August 2021; published 28 September 2021)

In the paper, the inclusive production of heavy quarkonium η_Q ($Q = b$ or c) via Z boson decays within the framework of nonrelativistic QCD effective theory are studied. The contributions from the leading color-singlet and color-octet Fock states are considered. Total and differential decay widths for the inclusive decays $Z \rightarrow \eta_Q + X$ are presented. It is found that the decays $Z \rightarrow \eta_Q + X$ are dominated by the ${}^3S_1^{[8]}$ component, so the decays can be inversely adopted to determine the values of the long-distance matrix elements $\langle \mathcal{O}^{n_c}({}^3S_1^{[8]}) \rangle$ and $\langle \mathcal{O}^{n_b}({}^3S_1^{[8]}) \rangle$, respectively. Our numerical results show that at an e^+e^- collider running at the Z pole with a high luminosity around $10^{35} \text{ cm}^{-2} \text{ s}^{-1}$ (a super Z factory), there are about 4.5×10^7 η_c meson events and 6.1×10^5 η_b meson events to be produced per operation year, and the inclusive decays may be used for clarifying some problems on the heavy quarkonium η_Q and nonrelativistic QCD.

DOI: [10.1103/PhysRevD.104.054044](https://doi.org/10.1103/PhysRevD.104.054044)

I. INTRODUCTION

Heavy quarkonia have attracted a lot of interest since the discovery of the J/ψ meson. An important reason is that they provide an ideal platform for studying the interplay between the perturbative and the nonperturbative effects in QCD. The nonrelativistic QCD (NRQCD) factorization formalism [1] provides a systematic framework to separate the short-distance and the long-distance effects in the heavy quarkonium production and decay processes. Under the NRQCD factorization, the heavy quarkonium production cross sections are expressed as the products of the short-distance coefficients (SDCs) and the long-distance matrix elements (LDMEs). The SDCs describe the production of

heavy quark-antiquark pairs with proper quantum numbers, which can be calculated perturbatively. The LDMEs describe the hadronization of a produced heavy quark pair into quarkonium, which are nonperturbative in nature but can be extracted from a global fit of experimental measurements or estimated by using the QCD inspired potential models etc.

Up to now, the NRQCD factorization formalism has achieved great successes in explaining the data at the high-energy colliders [2,3]. However, there are still some challenges. For instance, the global fits of the J/ψ color-octet (CO) LDMEs from various groups are not so consistent with each other, cf. Refs. [4–7]. Thus, it is interesting to study more quarkonium processes relating the NRQCD factorization formalism.

Most studies of the quarkonia focus on the J/ψ and Υ mesons due to their high detection efficiency. For instance, the J/ψ events can be reconstructed via the decays $J/\psi \rightarrow l^+l^-$ ($l = e, \mu$) with high efficiency, whose total branching ratio is $\sim 12\%$ [8]. Contrary to the J/ψ meson, there are less studies of the η_c meson production. Conventionally, the decay channel used to reconstruct the η_c events is $\eta_c \rightarrow \gamma\gamma$, and the branching ratio of this decay channel is $\sim 1.6 \times 10^{-4}$ [8]. Moreover, it is very difficult to record the two photons from the background in a hadron collision

*zhengxc@cqu.edu.cn

†zhangzx@itp.ac.cn

‡wuxg@cqu.edu.cn

§hxud@cqu.edu.cn

||gywang@cqu.edu.cn

Published by the American Physical Society under the terms of the Creative Commons Attribution 4.0 International license. Further distribution of this work must maintain attribution to the author(s) and the published article's title, journal citation, and DOI. Funded by SCOAP³.

environment. Namely the experimental detection of the η_c meson is poor. A novel proposal to reconstruct the η_c events through the decay channel $\eta_c \rightarrow p\bar{p}$ has been suggested in Ref. [9], whose branching ratio is $\sim 1.5 \times 10^{-3}$.¹ This proposal opened a new way to study the η_c meson at the high-energy colliders, and it has been adopted to observe the η_c meson by the LHCb Collaboration [10,11]. Recent theoretical studies of the η_c production at the LHC can be found in Refs. [12–20].

The η_b meson has the same quantum numbers as those of the η_c meson, but has different constituent quark mass. Since the heavier bottom quark mass, the η_b meson is a better object for applying NRQCD. Thus it is interesting to study the η_b and η_c production applying the NRQCD factorization at the same time, although the observations on the η_b are scarce. Up to now, the η_b has been observed only through the feed-down contributions, i.e., from the decays of excited bottomonium states. Therefore, the studies of the η_b production from various processes are requested.

At the LHC or an e^+e^- collider running around the Z pole and with an accessible high-luminosity (a super Z factory), the production of the heavy quarkonium η_Q through Z boson decays can provide abundant information. The inclusive Z boson production cross section at the LHC with the collision energy 13 TeV is ~ 56 nb [21]. With the luminosity of 10^{34} cm⁻² s⁻¹, there are $\sim 5.6 \times 10^9$ Z bosons to be produced per operation year at the LHC. A Chinese group has proposed to build a super Z factory [22], and its luminosity of the super Z factory could reach to 10^{34-36} cm⁻² s⁻¹, which is higher than that of the LEP-I by three to five orders. The Z boson production cross section is ~ 30 nb, and there are about $3 \times 10^{9-11}$ Z bosons to be produced per operation year at the super Z factory. Therefore, it is interesting to study the production of heavy quarkonia through Z boson decays.

The production of heavy quarkonia (J/ψ and Υ etc) through Z decays has been extensively studied at the leading order in α_s and v_Q [23–30], the typical velocity of the heavy quark in quarkonia. For the J/ψ and Υ production through Z boson decays, the CO contributions have been estimated in Refs. [31–34], the next-to-leading-order (NLO) QCD corrections have been calculated in Ref. [35], and the leading and next-to-leading logarithms of m_Z/m_Q have been resummed through the fragmentation approach in Ref. [36]. In the present paper, we devote ourselves to studying the inclusive production of η_Q with $Q = c$ or b through the Z boson decays.

¹In fact, the decay channels $\eta_c \rightarrow \Lambda\bar{\Lambda}$ and $\eta_c \rightarrow \Sigma\bar{\Sigma}$, whose branching ratios are $\sim 1.07 \times 10^{-3}$ and $\sim 2.1 \times 10^{-3}$, respectively [8], may also be used to identify the η_c meson so as to increase the detection efficiency of η_c . It is not very difficult to detect the strange baryon pairs produced from the η_c decay with vertex detectors because they carry high momentum from the η_c and make tracks.

According to NRQCD, for the η_Q production, the leading color-singlet (CS) and color-octet (CO) Fock states are $^1S_0^{[1]}$ at v_Q^3 order and $^1S_0^{[8]}$, $^3S_1^{[8]}$, and $^1P_1^{[8]}$ at v_Q^4 order. Although the CO contributions are suppressed by v_Q^4 order compared to the CS contribution in the long-distance part, the CO contributions may be enhanced in the short-distance part. Therefore, besides the CS state $^1S_0^{[1]}$, we also consider the CO states $^1S_0^{[8]}$, $^3S_1^{[8]}$, and $^1P_1^{[8]}$.

The remaining parts of the paper are organized as follows. In Sec. II, we briefly present the useful formulas for calculating the $Z \rightarrow \eta_Q$ inclusive decays. In Sec. III, numerical results are presented. Section IV is reserved for discussion and conclusion.

II. CALCULATION TECHNOLOGY

Under the NRQCD factorization formalism, the decay width for the inclusive process $Z \rightarrow \eta_Q + X$ can be written as

$$d\Gamma_{Z \rightarrow \eta_Q + X} = \sum_n d\tilde{\Gamma}_{Z \rightarrow (Q\bar{Q})[n] + X} \langle \mathcal{O}^{\eta_Q}(n) \rangle, \quad (1)$$

where $d\tilde{\Gamma}$ are the perturbatively calculable SDCs and $\langle \mathcal{O}^{\eta_Q}(n) \rangle$ are the nonperturbative LDMEs. The sum extends over the intermediate states $^{2S+1}L_J^{[1,8]}$. Up to relative v_Q^4 order, the LDMEs $\langle \mathcal{O}^{\eta_Q}(^1S_0^{[1]}) \rangle$, $\langle \mathcal{O}^{\eta_Q}(^1S_0^{[8]}) \rangle$, $\langle \mathcal{O}^{\eta_Q}(^3S_1^{[8]}) \rangle$, and $\langle \mathcal{O}^{\eta_Q}(^1P_1^{[8]}) \rangle$ are involved.

To calculate the decay width for $Z \rightarrow \eta_Q + X$, we first calculate the decay widths for a free on shell $(Q\bar{Q})$ pair with the quantum numbers $^{2S+1}L_J^{[1,8]}$, i.e., $d\Gamma_{Z \rightarrow (Q\bar{Q})[^{2S+1}L_J^{[1,8]}] + X}$. Then the contributions of different channels to the decay width of the $Z \rightarrow \eta_Q + X$ are obtained from $d\Gamma_{Z \rightarrow (Q\bar{Q})[^{2S+1}L_J^{[1,8]}] + X}$ through replacing the matrix element $\langle \mathcal{O}(Q\bar{Q})[^{2S+1}L_J^{[1,8]}](^{2S+1}L_J^{[1,8]}) \rangle$ by $\langle \mathcal{O}^{\eta_Q}(^{2S+1}L_J^{[1,8]}) \rangle$.

In the paper, we consider the contributions from the processes up to $\alpha\alpha_s^2$ order. The involved decay channels are

$$Z \rightarrow \eta_Q(^1S_0^{[8]}, ^3S_1^{[8]}, ^1P_1^{[8]}) + g, \quad (2)$$

$$Z \rightarrow \eta_Q(^1S_0^{[1]}, ^1S_0^{[8]}, ^3S_1^{[8]}, ^1P_1^{[8]}) + gg, \quad (3)$$

$$Z \rightarrow \eta_Q(^1S_0^{[8]}, ^3S_1^{[8]}, ^1P_1^{[8]}) + q\bar{q}, \quad (4)$$

$$Z \rightarrow \eta_Q(^1S_0^{[1]}, ^1S_0^{[8]}, ^3S_1^{[8]}, ^1P_1^{[8]}) + Q\bar{Q}, \quad (5)$$

$$Z \rightarrow \eta_Q(^1S_0^{[8]}, ^3S_1^{[8]}, ^1P_1^{[8]}) + Q'\bar{Q}'(Q' \neq Q). \quad (6)$$

The decay channels $Z \rightarrow \eta_Q(^1S_0^{[8]}, ^3S_1^{[8]}, ^1P_1^{[8]}) + gg$ and $Z \rightarrow \eta_Q(^1S_0^{[8]}, ^3S_1^{[8]}, ^1P_1^{[8]}) + q\bar{q}$ are the real corrections to

the decay channels $Z \rightarrow \eta_Q(^1S_0^{[8]}, ^3S_1^{[8]}, ^1P_1^{[8]}) + g$, and should be considered together with the virtual corrections to the decay channels $Z \rightarrow \eta_Q(^1S_0^{[8]}, ^3S_1^{[8]}, ^1P_1^{[8]}) + g$ so as to obtain finite predictions.

The decay width for the $(Q\bar{Q})^{[2S+1]L_J^{[1,8]}}$ pair can be written as

$$d\Gamma_{Z \rightarrow (Q\bar{Q})^{[2S+1]L_J^{[1,8]}} + X} = \frac{1}{3} \frac{1}{2m_Z} \sum |\mathcal{M}|^2 d\Phi_N, \quad (7)$$

where N indicates that there are N particles in the final state, \sum indicates the sum over the spin and color states of initial and final particles, and $1/3$ comes from the polarization average of the initial Z boson. $d\Phi_N$ is N -body differential phase space

$$d\Phi_N = (2\pi)^4 \delta^4\left(p_0 - \sum_{f=1}^N p_f\right) \prod_{f=1}^N \frac{d^3\mathbf{p}_f}{(2\pi)^3 2E_f}, \quad (8)$$

and \mathcal{M} denotes the amplitude for the $(Q\bar{Q})^{[2S+1]L_J^{[1,8]}}$ pair. In the following, we sketch the formulas used in the calculation of these decay channels, successively.

A. $Z \rightarrow \eta_Q(^1S_0^{[8]}, ^3S_1^{[8]}, ^1P_1^{[8]}) + g$ and their NLO QCD corrections

1. Leading order contributions

At leading order (LO) in α_s , there are two Feynman diagrams for the decay channel $Z \rightarrow (Q\bar{Q})^{[2S+1]L_J^{[8]}} + g$, which are shown in Fig. 1. The amplitude ($\mathcal{M} = \mathcal{M}_1 + \mathcal{M}_2$) for the decay channel can be written down according to the two Feynman diagrams. For the $^1S_0^{[8]}$ ($^3S_1^{[8]}$) case, we have

$$i\mathcal{M}_1 = -\frac{ig}{2\cos\theta_W} \text{tr} \left[\Pi_{1(3)} \Lambda_8^a \not{\epsilon}(p_0) (V_Q - A_Q \gamma_5) \cdot \frac{i}{-\not{p}_{12} - \not{p}_2 - m_Q + i\epsilon} (ig_s \not{\epsilon}^*(p_2) T^b) \right] \Bigg|_{q=0}, \quad (9)$$

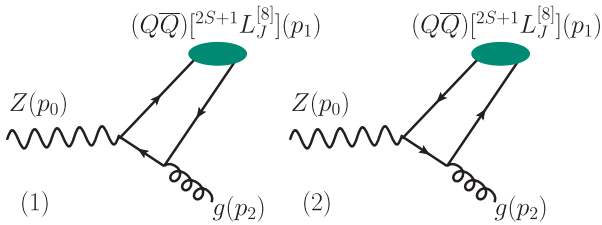


FIG. 1. Feynman diagrams for $Z \rightarrow (Q\bar{Q})^{[2S+1]L_J^{[8]}} + g$.

$$i\mathcal{M}_2 = -\frac{ig}{2\cos\theta_W} \text{tr} \left[\Pi_{1(3)} \Lambda_8^a (ig_s \not{\epsilon}^*(p_2) T^b) \cdot \frac{i}{\not{p}_{11} + \not{p}_2 - m_Q + i\epsilon} \not{\epsilon}(p_0) (V_Q - A_Q \gamma_5) \right] \Bigg|_{q=0}, \quad (10)$$

where V_Q and A_Q are vector and axial electroweak couplings. More explicitly, $V_Q = T_{3Q} - 2e_Q \sin^2 \theta_W$ and $A_Q = T_{3Q}$, where T_{3Q} and e_Q are weak isospin and the charge of fermion Q in units of positron charge, respectively. $p_{11} = p_1/2 + q$ and $p_{12} = p_1/2 - q$ are the momenta of the Q and \bar{Q} in the $(Q\bar{Q})^{[2S+1]L_J^{[8]}}$ pair, and $\Pi_{1(3)}$ is the spin-singlet (spin-triplet) projector, i.e.,

$$\Pi_1 = \frac{1}{(2m_Q)^{3/2}} (\not{p}_{12} - m_Q) \gamma_5 (\not{p}_{11} + m_Q), \quad (11)$$

$$\Pi_3 = \frac{1}{(2m_Q)^{3/2}} (\not{p}_{12} - m_Q) \not{\epsilon}^*(p_1) (\not{p}_{11} + m_Q), \quad (12)$$

and $\Lambda_8^a = \sqrt{2} T^a$ is the CO projector. For the $^1P_1^{[8]}$ case, we have

$$i\mathcal{M}_1 = -\frac{ig\epsilon_a^*(p_1)}{2\cos\theta_W} \frac{d}{dq_\alpha} \text{tr} \left[\Pi_1 \Lambda_8^a \not{\epsilon}(p_0) (V_Q - A_Q \gamma_5) \cdot \frac{i}{-\not{p}_{12} - \not{p}_2 - m_Q + i\epsilon} (ig_s \not{\epsilon}^*(p_2) T^b) \right] \Bigg|_{q=0}, \quad (13)$$

$$i\mathcal{M}_2 = -\frac{ig\epsilon_a^*(p_1)}{2\cos\theta_W} \frac{d}{dq_\alpha} \text{tr} \left[\Pi_1 \Lambda_8^a (ig_s \not{\epsilon}^*(p_2) T^b) \cdot \frac{i}{\not{p}_{11} + \not{p}_2 - m_Q + i\epsilon} \not{\epsilon}(p_0) (V_Q - A_Q \gamma_5) \right] \Bigg|_{q=0}. \quad (14)$$

Squaring the amplitude \mathcal{M} and integrating the squared amplitude over the two-body phase space, we obtain the LO contribution for the decay channel $Z \rightarrow (Q\bar{Q})^{[2S+1]L_J^{[8]}} + g$.

2. Virtual corrections

The NLO virtual corrections come from the interference of the one-loop diagrams and the LO diagrams. Four sample one-loop Feynman diagrams are shown in Fig. 2. The fourth sample Feynman diagram is specific to the $^3S_1^{[8]}$ channel. The amplitude is too lengthy to be listed here.

There are UV divergences in the self-energy and vertex diagrams and IR divergences in the vertex and box diagrams. We adopt dimensional regularization with $d = 4 - 2\epsilon$ to regularize these divergences. Then the divergences appear as pole terms in ϵ . The γ_5 matrix should be noted in dimensional regularization, and we adopt the reading point prescription [37] to deal with it.

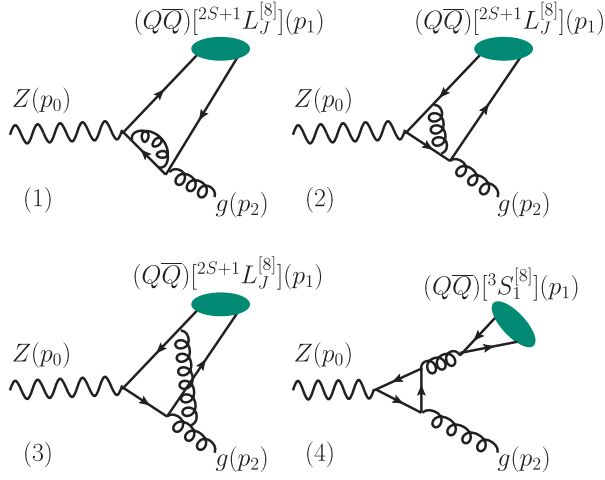


FIG. 2. Four sample Feynman diagrams for the virtual corrections to $Z \rightarrow (Q\bar{Q})^{[2S+1]L_J^{[8]}} + g$.

The UV divergences should be removed through renormalization. In the calculation, the renormalization scheme is adopted as follows: the renormalization of the quark field, the quark mass and the gluon field is carried out in the on-mass-shell (OS) scheme, while the renormalization of the strong coupling constant is carried out in the modified minimal subtraction ($\overline{\text{MS}}$) scheme. The renormalization constants are

$$\delta Z_{2,Q}^{\text{OS}} = -C_F \frac{\alpha_s}{4\pi} \left[\frac{1}{\epsilon_{UV}} + \frac{2}{\epsilon_{IR}} - 3\gamma_E + 3 \ln \frac{4\pi\mu_R^2}{m_Q^2} + 4 \right],$$

$$\delta Z_{m,Q}^{\text{OS}} = -3C_F \frac{\alpha_s}{4\pi} \left[\frac{1}{\epsilon_{UV}} - \gamma_E + \ln \frac{4\pi\mu_R^2}{m_Q^2} + \frac{4}{3} \right],$$

$$\delta Z_3^{\text{OS}} = \frac{\alpha_s}{4\pi} \left[(\beta'_0 - 2C_A) \left(\frac{1}{\epsilon_{UV}} - \frac{1}{\epsilon_{IR}} \right) - \frac{4}{3} T_F \sum_Q \left(\frac{1}{\epsilon_{UV}} - \gamma_E + \ln \frac{4\pi\mu_R^2}{m_Q^2} \right) \right],$$

$$\delta Z_g^{\overline{\text{MS}}} = -\frac{\beta_0}{2} \frac{\alpha_s}{4\pi} \left[\frac{1}{\epsilon_{UV}} - \gamma_E + \ln(4\pi) \right],$$

where γ_E is the Euler constant, μ_R is the renormalization scale, $\beta_0 = 11 - 2n_f/3$ is the one-loop coefficient of the QCD β function, and n_f is the flavor number of active quarks. $\beta'_0 = 11 - 2n_{lf}/3$ and $n_{lf} = 3$ is the number of light-quark flavors. For $SU(3)$ group, $C_F = 4/3$, $T_F = 1/2$, and $C_A = 3$.

In the calculation, the threshold expansion method [38] is employed to extract the SDCs; i.e., we expand the relative momentum (q) of the $(Q\bar{Q})^{[2S+1]L_J^{[8]}}$ pair before performing the loop integration. Then the Coulomb divergences, which are IR power divergences and vanish in dimensional regularization, do not appear in our calculation.

3. Real corrections

The real corrections to the decay channel $Z \rightarrow (Q\bar{Q})^{[2S+1]L_J^{[8]}} + g$ come from the processes $Z \rightarrow (Q\bar{Q})^{[2S+1]L_J^{[8]}} + gg$ and $Z \rightarrow (Q\bar{Q})^{[2S+1]L_J^{[8]}} + q\bar{q}$, where $q = u, d, s$. In the calculation, we use $\sum_i \epsilon_i^{\mu*} \epsilon_i^\nu \rightarrow -g_{\mu\nu}$ to sum the polarizations of the final-state gluons. The unphysical polarization contributions are subtracted through the process involving ghost-pair production, i.e., $Z \rightarrow (Q\bar{Q})^{[2S+1]L_J^{[8]}} + u_g \bar{u}_g$. Six sample Feynman diagrams for the real corrections are shown in Fig. 3. The sixth diagram is specific to the ${}^3S_1^{[8]}$ channel.

There are IR divergences in the real corrections. These IR divergences should be regularized by dimensional regularization as those in the virtual corrections. In order to simplify the calculation of the real corrections under dimensional regularization, we adopt the two-cutoff phase-space slicing method [39] to isolate the divergent terms. Under this method, the differential decay width for the real corrections can be decomposed into three parts,

$$d\Gamma_{\text{Real}} = d\Gamma_S + d\Gamma_{\text{HC}} + d\Gamma_{\text{HC}}, \quad (15)$$

where $d\Gamma_S$ denotes the contribution from the phase space region with $E_2 \leq m_Z \delta_s/2$ or $E_3 \leq m_Z \delta_s/2$, $d\Gamma_{\text{HC}}$ denotes the contribution from the phase space region with $E_2 > m_Z \delta_s/2$, $E_3 > m_Z \delta_s/2$ and $(p_2 + p_3)^2 \leq m_Z^2 \delta_c$, and Γ_{HC} denotes the contribution from the phase space region with $E_2 > m_Z \delta_s/2$, $E_3 > m_Z \delta_s/2$, and

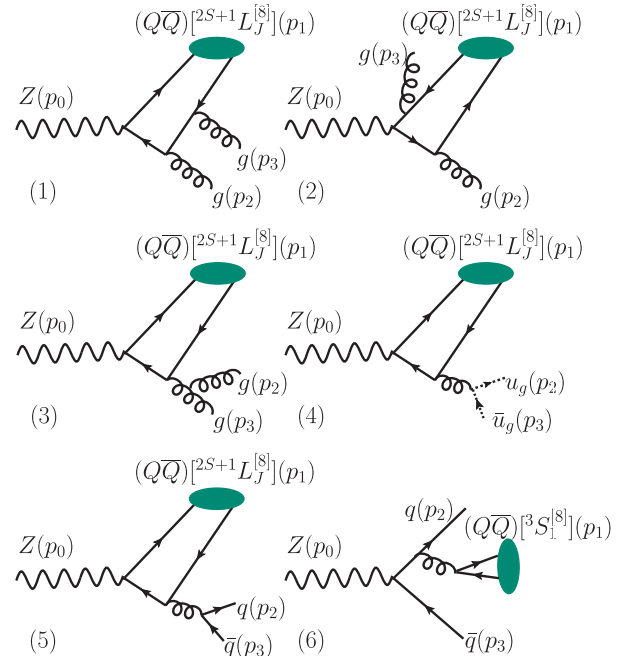


FIG. 3. Six sample Feynman diagrams for the real corrections to $Z \rightarrow (Q\bar{Q})^{[2S+1]L_J^{[8]}} + g$.

$(p_2 + p_3)^2 > m_Z^2 \delta_c$. In the calculation, the two cutoff parameters should be taken as $\delta_c \ll \delta_s \ll 1$. Applying the eikonal and collinear approximations to the soft and hard-collinear parts, respectively, Γ_S and Γ_{HC} can be calculated analytically in d space-time dimensions. Due to the constraints $E_2 > m_Z \delta_s / 2$, $E_3 > m_Z \delta_s / 2$ and $(p_2 + p_3)^2 > m_Z^2 \delta_c$, Γ_{HC} is finite and can be calculated in four space-time dimensions safely.

After summing the virtual and real corrections, the IR divergences are canceled in the $1S_0^{[8]}$ and $3S_1^{[8]}$ cases. However, there are IR divergences remaining in the $1P_1^{[8]}$ case after summing the virtual and real corrections. The finite SDC for the $1P_1^{[8]}$ channel can be extracted through matching.

Applying the NRQCD factorization to the production of an on shell $(Q\bar{Q})[1P_1^{[8]}]$ pair, the decay width can be written as

$$\begin{aligned}
 d\Gamma_{1P_1^{[8]}} &= d\tilde{\Gamma}_{1P_1^{[8]}} \langle \mathcal{O}(Q\bar{Q})[1P_1^{[8]}](1P_1^{[8]}) \rangle \\
 &\quad + d\tilde{\Gamma}_{1S_0^{[1]}} \langle \mathcal{O}(Q\bar{Q})[1P_1^{[8]}](1S_0^{[1]}) \rangle \\
 &\quad + d\tilde{\Gamma}_{1S_0^{[8]}} \langle \mathcal{O}(Q\bar{Q})[1P_1^{[8]}](1S_0^{[8]}) \rangle, \quad (16)
 \end{aligned}$$

where $d\Gamma_{1P_1^{[8]}}$ denotes the decay width for an on shell $(Q\bar{Q})$ pair with quantum numbers $1P_1^{[8]}$, $\langle \mathcal{O}(Q\bar{Q})[1P_1^{[8]}](^{2S+1}L_J^{[8]}) \rangle$ denotes the LDMEs for the quark pair. The LDME $\langle \mathcal{O}(Q\bar{Q})[1P_1^{[8]}](1P_1^{[8]}) \rangle$ starts at α_s^0 order, while $\langle \mathcal{O}(Q\bar{Q})[1P_1^{[8]}](1S_0^{[1]}) \rangle$ and $\langle \mathcal{O}(Q\bar{Q})[1P_1^{[8]}](1S_0^{[8]}) \rangle$ start at α_s order. Up to α_s^2 order, the second term vanishes in this decay channel. Then, we have

$$\begin{aligned}
 d\tilde{\Gamma}_{1P_1^{[8]}} &= \frac{d\Gamma_{1P_1^{[8]}}}{\langle \mathcal{O}(Q\bar{Q})[1P_1^{[8]}](1P_1^{[8]}) \rangle} \\
 &\quad - \frac{d\tilde{\Gamma}_{1S_0^{[8]}} \langle \mathcal{O}(Q\bar{Q})[1P_1^{[8]}](1S_0^{[8]}) \rangle}{\langle \mathcal{O}(Q\bar{Q})[1P_1^{[8]}](1P_1^{[8]}) \rangle}. \quad (17)
 \end{aligned}$$

Under the $\overline{\text{MS}}$ factorization scheme,

$$\langle \mathcal{O}(Q\bar{Q})[1P_1^{[8]}](1S_0^{[8]}) \rangle = -\frac{\alpha_s B_F C_\epsilon}{3\pi m_Q^2} \langle \mathcal{O}(Q\bar{Q})[1P_1^{[8]}](1P_1^{[8]}) \rangle, \quad (18)$$

where $B_F = (N_c^2 - 4)/N_c$ and $C_\epsilon = 1/\epsilon_{IR} - \gamma_E + \ln(4\pi) + \ln(\mu_R^2/\mu_\Lambda^2)$. Then the finite SDC $d\tilde{\Gamma}_{1P_1^{[8]}}$ is obtained.

B. $Z \rightarrow \eta_Q(1S_0^{[1]}, 1S_0^{[8]}, 3S_1^{[8]}, 1P_1^{[8]}) + Q\bar{Q}$

For the CS decay channel $Z \rightarrow (Q\bar{Q})[1S_0^{[1]}] + Q\bar{Q}$, there are four Feynman diagrams which are shown in Fig. 4. The amplitude ($\mathcal{M} = \sum_{i=1}^4 \mathcal{M}_i$) can be written down according to the four Feynman diagrams,

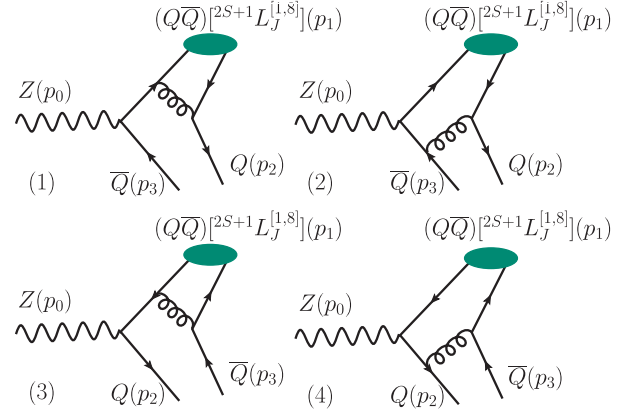


FIG. 4. Four of the Feynman diagrams for $Z \rightarrow (Q\bar{Q})[^{2S+1}L_J^{[1,8]}] + Q\bar{Q}$.

$$\begin{aligned}
 i\mathcal{M}_1 &= -\frac{ig}{2\cos\theta_W} \frac{-i}{(p_{12} + p_2)^2 + i\epsilon} \bar{u}(p_2) (ig_s \gamma^\mu T^b) \\
 &\quad \cdot \Pi_1 \Lambda_1 (ig_s \gamma_\mu T^b) \frac{i}{\not{p}_1 + \not{p}_2 - m_Q + i\epsilon} \not{p}(p_0) \\
 &\quad \cdot (V_Q - A_Q \gamma_5) v(p_3)|_{q=0}, \quad (19)
 \end{aligned}$$

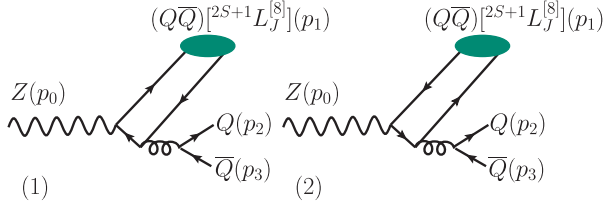
$$\begin{aligned}
 i\mathcal{M}_2 &= -\frac{ig}{2\cos\theta_W} \frac{-i}{(p_{12} + p_2)^2 + i\epsilon} \bar{u}(p_2) (ig_s \gamma^\mu T^b) \Pi_1 \\
 &\quad \cdot \Lambda_1 \not{p}(p_0) (V_Q - A_Q \gamma_5) \frac{i}{-\not{p}_0 + \not{p}_{11} - m_Q + i\epsilon} \\
 &\quad \cdot (ig_s \gamma_\mu T^b) v(p_3)|_{q=0}, \quad (20)
 \end{aligned}$$

$$\begin{aligned}
 i\mathcal{M}_3 &= -\frac{ig}{2\cos\theta_W} \frac{-i}{(p_{11} + p_3)^2 + i\epsilon} \bar{u}(p_2) \not{p}(p_0) \\
 &\quad \cdot (V_Q - A_Q \gamma_5) \frac{i}{-\not{p}_1 - \not{p}_3 - m_Q + i\epsilon} (ig_s \gamma_\mu T^b) \\
 &\quad \cdot \Pi_1 \Lambda_1 (ig_s \gamma^\mu T^b) v(p_3)|_{q=0}, \quad (21)
 \end{aligned}$$

$$\begin{aligned}
 i\mathcal{M}_4 &= -\frac{ig}{2\cos\theta_W} \frac{-i}{(p_{11} + p_3)^2 + i\epsilon} \bar{u}(p_2) (ig_s \gamma_\mu T^b) \\
 &\quad \cdot \frac{i}{\not{p}_0 - \not{p}_{12} - m_Q + i\epsilon} \not{p}(p_0) (V_Q - A_Q \gamma_5) \\
 &\quad \cdot \Pi_1 \Lambda_1 (ig_s \gamma^\mu T^b) v(p_3)|_{q=0}, \quad (22)
 \end{aligned}$$

where $\Lambda_1 = \mathbf{1}/\sqrt{3}$ is the CS projector.

For the decay channel $Z \rightarrow (Q\bar{Q})[1S_0^{[8]}] + Q\bar{Q}$, there are six Feynman diagrams which are shown in Figs. 4 and 5. The amplitude ($\mathcal{M} = \sum_{i=1}^6 \mathcal{M}_i$) can be written down according to the six Feynman diagrams. The amplitudes $\mathcal{M}_i (i = 1, 2, 3, 4)$ can be obtained from the amplitudes $\mathcal{M}_i (i = 1, 2, 3, 4)$ of $Z \rightarrow (Q\bar{Q})[1S_0^{[1]}] + Q\bar{Q}$ through the replacements $\Lambda_1 \rightarrow \Lambda_8$. And the remaining two amplitudes $\mathcal{M}_i (i = 5, 6)$ are as follows:


 FIG. 5. Two of the Feynman diagrams for $Z \rightarrow (Q\bar{Q}) [{}^{2S+1}L_J^{[8]}] + Q\bar{Q}$.

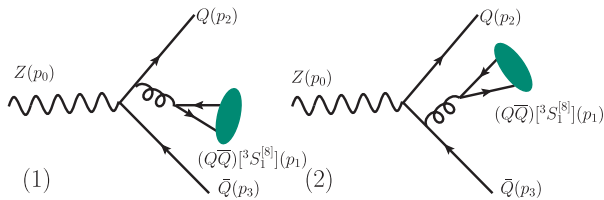
$$i\mathcal{M}_5 = \frac{ig}{2 \cos \theta_W} \frac{-i}{(p_2 + p_3)^2 + i\epsilon} \text{tr} \left[\Pi_1 \Lambda_8^a \not{\epsilon}(p_0) \right. \\ \left. \times (V_Q - A_Q \gamma_5) \frac{i}{-\not{p}_0 + \not{p}_{11} - m_Q + i\epsilon} (ig_s \gamma^\mu T^b) \right] \\ \times \bar{u}(p_2) (ig_s \gamma_\mu T^b) v(p_3) \Big|_{q=0}, \quad (23)$$

$$i\mathcal{M}_6 = \frac{ig}{2 \cos \theta_W} \frac{-i}{(p_2 + p_3)^2 + i\epsilon} \text{tr} \left[\Pi_1 \Lambda_8^a (ig_s \gamma^\mu T^b) \right. \\ \left. \times \frac{i}{\not{p}_0 - \not{p}_{12} - m_Q + i\epsilon} \not{\epsilon}(p_0) (V_Q - A_Q \gamma_5) \right] \\ \times \bar{u}(p_2) (ig_s \gamma_\mu T^b) v(p_3) \Big|_{q=0}. \quad (24)$$

There is an additional factor (-1) in $\mathcal{M}_i (i = 5, 6)$ compared to $\mathcal{M}_i (i = 1, 2, 3, 4)$, which is due to the fermion exchange.

For the decay channel $Z \rightarrow (Q\bar{Q}) [{}^3S_1^{[8]}] + Q\bar{Q}$, there are eight Feynman diagrams which are shown in Figs. 4–6. The amplitude can be written as $\mathcal{M} = \sum_{i=1}^8 \mathcal{M}_i$. The amplitudes $\mathcal{M}_i (i = 1, 2, 3, 4)$ can be obtained from Eqs. (19)–(22) through the replacement $\Pi_1 \rightarrow \Pi_3$ and $\Lambda_1 \rightarrow \Lambda_8$. The amplitudes $\mathcal{M}_i (i = 5, 6)$ can be obtained from Eqs. (23) and (24) through the replacement $\Pi_1 \rightarrow \Pi_3$. The other two amplitudes $\mathcal{M}_i (i = 7, 8)$ are as follows:

$$i\mathcal{M}_7 = \frac{ig}{2 \cos \theta_W} \frac{-i}{p_1^2 + i\epsilon} \text{tr} [\Pi_3 \Lambda_8^a (ig_s \gamma^\mu T^b)] \bar{u}(p_2) (ig_s \gamma_\mu T^b) \\ \cdot \frac{i}{\not{p}_1 + \not{p}_2 - m_Q + i\epsilon} \not{\epsilon}(p_0) (V_Q - A_Q \gamma_5) v(p_3) \Big|_{q=0}, \quad (25)$$


 FIG. 6. Two of the Feynman diagrams for $Z \rightarrow (Q\bar{Q}) [{}^3S_1^{[8]}] + Q\bar{Q}$.

$$i\mathcal{M}_8 = \frac{ig}{2 \cos \theta_W} \frac{-i}{p_1^2 + i\epsilon} \text{tr} [\Pi_3 \Lambda_8^a (ig_s \gamma^\mu T^b)] \bar{u}(p_2) \not{\epsilon}(p_0) \\ \cdot (V_Q - A_Q \gamma_5) \frac{i}{-\not{p}_1 - \not{p}_3 - m_Q + i\epsilon} \\ \times (ig_s \gamma_\mu T^b) v(p_3) \Big|_{q=0}. \quad (26)$$

For the decay channel $Z \rightarrow (Q\bar{Q}) [{}^1P_1^{[8]}] + Q\bar{Q}$, there are six Feynman diagrams which are shown in Figs. 4 and 5. The amplitude can be written as $\mathcal{M} = \sum_{i=1}^6 \mathcal{M}_i$, and

$$i\mathcal{M}_1 = -\frac{ig\epsilon_a^*(p_1)}{2 \cos \theta_W} \frac{d}{dq_\alpha} \left[\frac{-i}{(p_{12} + p_2)^2 + i\epsilon} \bar{u}(p_2) (ig_s \gamma^\mu T^b) \right. \\ \cdot \Pi_1 \Lambda_8^a (ig_s \gamma_\mu T^b) \frac{i}{\not{p}_1 + \not{p}_2 - m_Q + i\epsilon} \not{\epsilon}(p_0) \\ \left. \cdot (V_Q - A_Q \gamma_5) v(p_3) \right] \Big|_{q=0}, \quad (27)$$

$$i\mathcal{M}_2 = -\frac{ig\epsilon_a^*(p_1)}{2 \cos \theta_W} \frac{d}{dq_\alpha} \left[\frac{-i}{(p_{12} + p_2)^2 + i\epsilon} \bar{u}(p_2) (ig_s \gamma^\mu T^b) \right. \\ \cdot \Pi_1 \Lambda_8^a \not{\epsilon}(p_0) (V_Q - A_Q \gamma_5) \frac{i}{-\not{p}_0 + \not{p}_{11} - m_Q + i\epsilon} \\ \left. \cdot (ig_s \gamma_\mu T^b) v(p_3) \right] \Big|_{q=0}, \quad (28)$$

$$i\mathcal{M}_3 = -\frac{ig\epsilon_a^*(p_1)}{2 \cos \theta_W} \frac{d}{dq_\alpha} \left[\frac{-i}{(p_{11} + p_3)^2 + i\epsilon} \bar{u}(p_2) \not{\epsilon}(p_0) \right. \\ \cdot (V_Q - A_Q \gamma_5) \frac{i}{-\not{p}_1 - \not{p}_3 - m_Q + i\epsilon} (ig_s \gamma_\mu T^b) \\ \left. \cdot \Pi_1 \Lambda_8^a (ig_s \gamma^\mu T^b) v(p_3) \right] \Big|_{q=0}, \quad (29)$$

$$i\mathcal{M}_4 = -\frac{ig\epsilon_a^*(p_1)}{2 \cos \theta_W} \frac{d}{dq_\alpha} \left[\frac{-i}{(p_{11} + p_3)^2 + i\epsilon} \bar{u}(p_2) (ig_s \gamma_\mu T^b) \right. \\ \cdot \frac{i}{\not{p}_0 - \not{p}_{12} - m_Q + i\epsilon} \not{\epsilon}(p_0) (V_Q - A_Q \gamma_5) \\ \left. \cdot \Pi_1 \Lambda_8^a (ig_s \gamma^\mu T^b) v(p_3) \right] \Big|_{q=0}, \quad (30)$$

$$i\mathcal{M}_5 = \frac{ig\epsilon_a^*(p_1)}{2 \cos \theta_W} \frac{-i}{(p_2 + p_3)^2 + i\epsilon} \frac{d}{dq_\alpha} \text{tr} \left[\Pi_1 \Lambda_8^a \not{\epsilon}(p_0) \right. \\ \left. \times (V_Q - A_Q \gamma_5) \frac{i}{-\not{p}_0 + \not{p}_{11} - m_Q + i\epsilon} (ig_s \gamma^\mu T^b) \right] \\ \times \bar{u}(p_2) (ig_s \gamma_\mu T^b) v(p_3) \Big|_{q=0}, \quad (31)$$

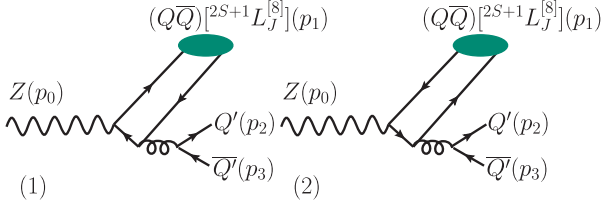


FIG. 7. Two of the Feynman diagrams for $Z \rightarrow (Q\bar{Q}) [{}^{2S+1}L_j^{[8]}] + Q'\bar{Q}'$.

$$i\mathcal{M}_6 = \frac{ig\epsilon_\alpha^*(p_1)}{2\cos\theta_W} \frac{-i}{(p_2 + p_3)^2 + i\epsilon} \frac{d}{dq_\alpha} \text{tr} \left[\Pi_1 \Lambda_8^a (ig_s \gamma^\mu T^b) \right. \\ \left. \times \frac{i}{\not{p}_0 - \not{p}_{12} - m_Q + i\epsilon} \not{\epsilon}(p_0) (V_Q - A_Q \gamma_5) \right] \\ \times \bar{u}(p_2) (ig_s \gamma_\mu T^b) v(p_3) \Big|_{q=0}. \quad (32)$$

C. $Z \rightarrow \eta_Q ({}^1S_0^{[8]}, {}^3S_1^{[8]}, {}^1P_1^{[8]}) + Q'\bar{Q}'$

In this subsection we present the amplitudes for the decay channels $Z \rightarrow \eta_Q ({}^1S_0^{[8]}, {}^3S_1^{[8]}, {}^1P_1^{[8]}) + Q'\bar{Q}'$ where Q' denotes a heavy quark but $Q' \neq Q$.

For the decay channel $Z \rightarrow (Q\bar{Q}) [{}^1S_0^{[8]}] + Q'\bar{Q}'$, there are two Feynman diagrams, which are shown in Fig. 7. The amplitude can be written as $\mathcal{M} = \mathcal{M}_1 + \mathcal{M}_2$. The amplitudes \mathcal{M}_1 and \mathcal{M}_2 are the same as \mathcal{M}_5 and \mathcal{M}_6 in Eqs. (23) and (24), but here we have $p_2^2 = p_3^2 = m_Q^2$.

For the decay channel $Z \rightarrow (Q\bar{Q}) [{}^3S_1^{[8]}] + Q'\bar{Q}'$, there are four Feynman diagrams, which are shown in Figs. 7 and 8. The amplitude can be written as $\mathcal{M} = \sum_{i=1}^4 \mathcal{M}_i$. The amplitudes \mathcal{M}_1 and \mathcal{M}_2 can be obtained from \mathcal{M}_5 and \mathcal{M}_6 in Eqs. (23) and (24) through replacement $\Pi_1 \rightarrow \Pi_3$. The amplitudes \mathcal{M}_3 and \mathcal{M}_4 , which correspond to the two diagrams in Fig. 8, are as follows:

$$i\mathcal{M}_3 = \frac{ig}{2\cos\theta_W} \frac{-i}{p_1^2 + i\epsilon} \text{tr} [\Pi_3 \Lambda_8^a (ig_s \gamma^\mu T^b)] \bar{u}(p_2) (ig_s \gamma_\mu T^b) \\ \cdot \frac{i}{\not{p}_1 + \not{p}_2 - m_{Q'} + i\epsilon} \not{\epsilon}(p_0) (V_{Q'} - A_{Q'} \gamma_5) v(p_3) \Big|_{q=0}, \quad (33)$$

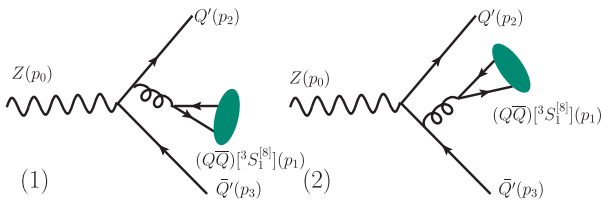


FIG. 8. Two of the Feynman diagrams for $Z \rightarrow (Q\bar{Q}) [{}^3S_1^{[8]}] + Q'\bar{Q}'$.

$$i\mathcal{M}_4 = \frac{ig}{2\cos\theta_W} \frac{-i}{p_1^2 + i\epsilon} \text{tr} [\Pi_3 \Lambda_8^a (ig_s \gamma^\mu T^b)] \bar{u}(p_2) \not{\epsilon}(p_0) \\ \times (V_{Q'} - A_{Q'} \gamma_5) \frac{i}{-\not{p}_1 - \not{p}_3 - m_{Q'} + i\epsilon} \\ \times (ig_s \gamma_\mu T^b) v(p_3) \Big|_{q=0}. \quad (34)$$

For the decay channel $Z \rightarrow (Q\bar{Q}) [{}^1P_1^{[8]}] + Q'\bar{Q}'$, there are two Feynman diagrams which are shown in Fig. 7. The amplitude can be written as $\mathcal{M} = \mathcal{M}_1 + \mathcal{M}_2$. The amplitudes \mathcal{M}_1 and \mathcal{M}_2 have the same form as \mathcal{M}_5 and \mathcal{M}_6 in Eqs. (31) and (32), but here $p_2^2 = p_3^2 = m_Q^2$.

D. $Z \rightarrow \eta_Q ({}^1S_0^{[1]}) + gg$

There are six Feynman diagrams for the decay channel $Z \rightarrow (Q\bar{Q}) [{}^1S_0^{[1]}] + gg$. Half of the Feynman diagrams are shown in Fig. 9, and the other three Feynman diagrams can be obtained from these diagrams through the substitution $p_2 \leftrightarrow p_3$. According to those diagrams, the amplitude ($\mathcal{M} = \sum_{i=1}^6 \mathcal{M}_i$) of the process can be written down, and we have

$$i\mathcal{M}_1 = -\frac{ig}{2\cos\theta_W} \text{tr} \left[\Pi_1 \Lambda_1 \not{\epsilon}(p_0) (V_Q - A_Q \gamma_5) \right. \\ \cdot \frac{i}{-\not{p}_0 + \not{p}_{11} - m_Q + i\epsilon} (ig_s \not{\epsilon}^*(p_3) T^b) \\ \left. \cdot \frac{i}{-\not{p}_2 - \not{p}_{12} - m_Q + i\epsilon} (ig_s \not{\epsilon}^*(p_2) T^a) \right] \Big|_{q=0}, \quad (35)$$

$$i\mathcal{M}_2 = -\frac{ig}{2\cos\theta_W} \text{tr} \left[\Pi_1 \Lambda_1 (ig_s \not{\epsilon}^*(p_2) T^a) \right. \\ \cdot \frac{i}{\not{p}_2 + \not{p}_{11} - m_Q + i\epsilon} \not{\epsilon}(p_0) (V_Q - A_Q \gamma_5) \\ \left. \cdot \frac{i}{-\not{p}_3 - \not{p}_{12} - m_Q + i\epsilon} (ig_s \not{\epsilon}^*(p_3) T^b) \right] \Big|_{q=0}, \quad (36)$$

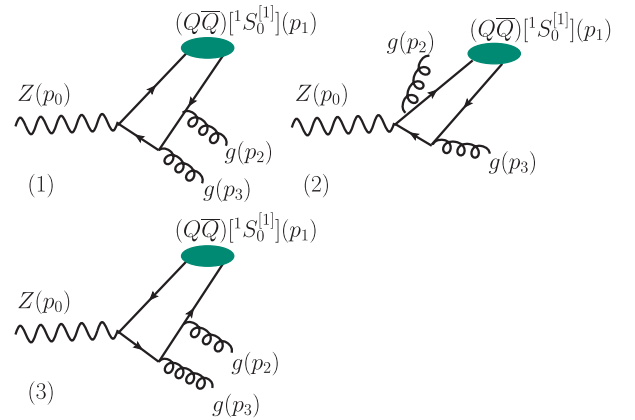


FIG. 9. Half of the Feynman diagrams for $Z \rightarrow (Q\bar{Q}) [{}^1S_0^{[1]}] + gg$.

TABLE I. The LDMEs for the J/ψ production extracted from the global fits, where $\mu_\Lambda = m_c$.

LDMEs	Butenschoen <i>et al.</i> [4]	Chao <i>et al.</i> [5]	Gong <i>et al.</i> [6]
$\langle \mathcal{O}^{J/\psi}(^3S_1^{[1]}) \rangle / \text{GeV}^3$	1.32	1.16	1.16
$\langle \mathcal{O}^{J/\psi}(^1S_0^{[8]}) \rangle / (10^{-2} \text{ GeV}^3)$	3.04	8.9	9.7
$\langle \mathcal{O}^{J/\psi}(^3S_1^{[8]}) \rangle / (10^{-2} \text{ GeV}^3)$	0.17	0.30	-0.46
$\langle \mathcal{O}^{J/\psi}(^3P_0^{[8]}) \rangle / (10^{-2} \text{ GeV}^5)$	-0.91	1.26	-2.14

$$\begin{aligned}
i\mathcal{M}_3 = & -\frac{ig}{2\cos\theta_W} \text{tr} \left[\Pi_1 \Lambda_1 (ig_s \not{\epsilon}^*(p_2) T^a) \right. \\
& \cdot \frac{i}{\not{p}_2 + \not{p}_{11} - m_Q + i\epsilon} (ig_s \not{\epsilon}^*(p_3) T^b) \\
& \left. \cdot \frac{i}{\not{p}_0 - \not{p}_{12} - m_Q + i\epsilon} \not{\epsilon}(p_0) (V_Q - A_Q \gamma_5) \right] \Bigg|_{q=0}.
\end{aligned} \quad (37)$$

The other three amplitudes M_i ($i = 4, 5, 6$) can be obtained from M_i ($i = 1, 2, 3$) via the substitution $p_2 \leftrightarrow p_3$.

III. NUMERICAL RESULTS

In the calculations, the package FeynArts [40] is employed to generate Feynman diagrams and amplitudes, the package FeynCalc [41,42] is employed to carry out the color and Dirac traces, the package \$Apart [43] is employed to conduct the partial fraction, the package FIRE [44] is employed to do the integration-by-parts reduction, and the package LoopTools [45] is used to compute the one-loop master integrals numerically. The phase-space integrations are performed by using the package VEGAS [46].

The necessary input parameters for the numerical calculation are taken as follows:

$$\begin{aligned}
m_c = 1.5 \text{ GeV}, \quad m_b = 4.75 \text{ GeV}, \quad m_Z = 91.1876 \text{ GeV}, \\
\sin^2\theta_W = 0.231, \quad \alpha = 1/128,
\end{aligned} \quad (38)$$

where α is the electromagnetic coupling constant at m_Z . For the strong coupling constant, we adopt the one-loop formula

$$\alpha_s(\mu_R) = \frac{4\pi}{\beta_0 \ln(\mu_R^2/\Lambda_{QCD}^2)}.$$

According to $\alpha_s(m_Z) = 0.1179$ [47], we obtain $\alpha_s(2m_c) = 0.234$ and $\alpha_s(2m_b) = 0.175$.

For the LDMEs, we derive the LDMEs for the η_Q from the experimentally extracted LDMEs for the J/ψ (Υ) via the heavy quark spin symmetry (HQSS), i.e.,

$$\begin{aligned}
\langle \mathcal{O}^{\eta_Q}(^1S_0^{[1]}/^1S_0^{[8]}) \rangle &= \frac{1}{3} \langle \mathcal{O}^{\psi_Q}(^3S_1^{[1]}/^3S_1^{[8]}) \rangle, \\
\langle \mathcal{O}^{\eta_Q}(^3S_1^{[8]}) \rangle &= \langle \mathcal{O}^{\psi_Q}(^1S_0^{[8]}) \rangle, \\
\langle \mathcal{O}^{\eta_Q}(^1P_1^{[8]}) \rangle &= 3 \langle \mathcal{O}^{\psi_Q}(^3P_0^{[8]}) \rangle.
\end{aligned} \quad (39)$$

These relations are expected to hold to relative order v_Q^2 . Several sets of the LDMEs for the J/ψ and the Υ extracted from the global fits by several groups are listed in Tables I and II. The factorization scale of the LDMEs has been taken as $\mu_\Lambda = 1.5 \text{ GeV}$ for the J/ψ and the Υ in Tables I and II. Thus, we also take this value for μ_Λ in this paper.

A. Integrated decay widths

In this subsection, we give the decay widths for different decay channels and the total decay widths for the inclusive η_Q production via Z boson decays.

The decay widths for the decay channels contributing to $Z \rightarrow \eta_c + X$ are given in Tables III–VI. In Table III, the decay widths for the decay channels $Z \rightarrow \eta_c(^{2S+1}L_J^{[8]}) + g$ up to LO and NLO accuracy in α_s are presented. We can see that the NLO correction is larger than the LO contribution in the $^1S_0^{[8]}$ and $^3S_1^{[8]}$ cases. The reason of the large NLO correction in the $^1S_0^{[8]}$ case is that only the vector coupling of the $Z - c\bar{c}$ vertex contributes to the decay width of $Z \rightarrow \eta_c(^1S_0^{[8]}) + g$ at the LO level, while both the vector and axial-vector couplings of the $Z - c\bar{c}$ vertex contribute to the NLO correction through the real corrections. Moreover, the strength of the axial-vector coupling is stronger than that of the vector coupling in the $Z - c\bar{c}$ vertex. Thus, the large NLO correction in the $^1S_0^{[8]}$ case is expected. The reason for

TABLE II. The LDMEs for the Υ production extracted from the global fits, where $\mu_\Lambda = 1.5 \text{ GeV}$.

LDMEs	Gong <i>et al.</i> [48]	Feng <i>et al.</i> [49]
$\langle \mathcal{O}^\Upsilon(^3S_1^{[1]}) \rangle / \text{GeV}^3$	9.28	9.28
$\langle \mathcal{O}^\Upsilon(^1S_0^{[8]}) \rangle / (10^{-2} \text{ GeV}^3)$	11.15	13.6
$\langle \mathcal{O}^\Upsilon(^3S_1^{[8]}) \rangle / (10^{-2} \text{ GeV}^3)$	-0.41	0.61
$\langle \mathcal{O}^\Upsilon(^3P_0^{[8]}) \rangle / m_b^2 / (10^{-2} \text{ GeV}^3)$	-0.67	-0.93

TABLE III. The decay widths (unit:keV) for the decay channels $Z \rightarrow \eta_c(2S+1L_J^{[8]}) + g$ based on three sets of LDMEs, where ‘‘NLO’’ denotes the results up to NLO accuracy. The very large NLO correction in the ${}^3S_1^{[8]}$ case comes from the contribution of the real correction processes $Z \rightarrow \eta_c({}^3S_1^{[8]}) + q\bar{q}$.

Decay channels	Butenschoen <i>et al.</i>	Chao <i>et al.</i>	Gong <i>et al.</i>
$\eta_c({}^1S_0^{[8]}) + g(\text{LO})$	3.29×10^{-3}	5.80×10^{-3}	-8.90×10^{-3}
$\eta_c({}^1S_0^{[8]}) + g(\text{NLO})$	1.79×10^{-2}	3.15×10^{-2}	-4.83×10^{-2}
$\eta_c({}^3S_1^{[8]}) + g(\text{LO})$	0.399	1.17	1.27
$\eta_c({}^3S_1^{[8]}) + g(\text{NLO})$	396	1.16×10^3	1.26×10^3
$\eta_c({}^1P_1^{[8]}) + g(\text{LO})$	-0.159	0.221	-0.375
$\eta_c({}^1P_1^{[8]}) + g(\text{NLO})$	-0.263	0.364	-0.618
Total($\eta_c + g$)(LO)	0.243	1.40	0.886
Total($\eta_c + g$)(NLO)	396	1.16×10^3	1.26×10^3

TABLE IV. The decay widths (unit:keV) for the decay channels $Z \rightarrow \eta_c(2S+1L_J^{[1,8]}) + c\bar{c}$ based on three sets of LDMEs.

Decay channels	Butenschoen <i>et al.</i>	Chao <i>et al.</i>	Gong <i>et al.</i>
$\eta_c({}^1S_0^{[1]}) + c\bar{c}$	90.9	79.9	79.9
$\eta_c({}^1S_0^{[8]}) + c\bar{c}$	1.10×10^{-2}	1.94×10^{-2}	-2.98×10^{-2}
$\eta_c({}^3S_1^{[8]}) + c\bar{c}$	104	305	332
$\eta_c({}^1P_1^{[8]}) + c\bar{c}$	-8.84×10^{-2}	0.122	-0.208
Total($\eta_c + c\bar{c}$)	195	385	412

TABLE V. The decay widths (unit:keV) for the decay channels $Z \rightarrow \eta_c(2S+1L_J^{[8]}) + b\bar{b}$ based on three sets of LDMEs.

Decay channels	Butenschoen <i>et al.</i>	Chao <i>et al.</i>	Gong <i>et al.</i>
$\eta_c({}^1S_0^{[8]}) + b\bar{b}$	8.53×10^{-5}	1.51×10^{-4}	-2.31×10^{-4}
$\eta_c({}^3S_1^{[8]}) + b\bar{b}$	117	342	373
$\eta_c({}^1P_1^{[8]}) + b\bar{b}$	-3.15×10^{-3}	4.36×10^{-3}	-7.40×10^{-3}
Total($\eta_c + b\bar{b}$)	117	342	373

the very large NLO correction in the ${}^3S_1^{[8]}$ case is that there are gluon fragmentation diagrams for the processes $Z \rightarrow \eta_c({}^3S_1^{[8]}) + q\bar{q}$ at $\alpha\alpha_s^2$ order. One of the gluon fragmentation diagram is the sixth diagram in Fig. 3. The decay width for $Z \rightarrow \eta_c({}^3S_1^{[8]}) + q\bar{q}$ ($q = u, d, s$)² is 1.15×10^3 keV under the LDME extracted by Chao *et al.*, which is very close to the decay width for $Z \rightarrow \eta_c({}^3S_1^{[8]}) + g$ at the NLO level.

²When we present the results for $Z \rightarrow \eta_Q({}^3S_1^{[8]}) + q\bar{q}$ individually, we actually give the contribution from the fragmentation diagrams, which is gauge invariant and counts almost the whole contribution of the NLO decay width of $Z \rightarrow \eta_c({}^3S_1^{[8]}) + g$.

TABLE VI. The decay width (unit:keV) for the decay channel $Z \rightarrow \eta_c({}^1S_0^{[1]}) + gg$ based on three sets of LDMEs.

Decay channels	Butenschoen <i>et al.</i>	Chao <i>et al.</i>	Gong <i>et al.</i>
$\eta_c({}^1S_0^{[1]}) + gg$	4.43	3.89	3.89

TABLE VII. The decay width (unit:MeV) for $Z \rightarrow \eta_c + X$ based on three sets of LDMEs.

	Butenschoen <i>et al.</i>	Chao <i>et al.</i>	Gong <i>et al.</i>
$\eta_c + X$	0.712	1.89	2.05

From these tables, we can see that the dominant contributions come from the decay channels $Z \rightarrow \eta_c({}^1S_0^{[1]}, {}^3S_1^{[8]}) + c\bar{c}$, $Z \rightarrow \eta_c({}^3S_1^{[8]}) + b\bar{b}$ and $Z \rightarrow \eta_c({}^3S_1^{[8]}) + q\bar{q}$. Among these dominant channels, the CO (${}^3S_1^{[8]}$) channels are more important than the CS (${}^1S_0^{[1]}$) channel under the three sets of LDMEs. The LO contributions from the decay channels associated with a final gluon are suppressed although they are of order $\alpha\alpha_s$.

These dominant decay channels can be understood by the fragmentation mechanism. For the decay channel $Z \rightarrow \eta_c({}^1S_0^{[1]}) + c\bar{c}$, the decay width is dominated by the (anti)quark fragmentation process of $Z \rightarrow c\bar{c}$ followed by $c(\bar{c}) \rightarrow \eta_c$. In this fragmentation process, the quark propagator is of order $1/m_{\eta_c}$, and the gluon propagator is of order $1/m_{\eta_c}^2$. For the decay channels $Z \rightarrow \eta_c({}^1S_0^{[8]}, {}^1P_1^{[8]}) + c\bar{c}$, the decay widths are also dominated by the (anti)quark fragmentation process. However, the involved LDMEs in the two decay channels are suppressed by powers of v_c compared with the CS LDME. Thus, the decay widths of the decay channels $Z \rightarrow \eta_c({}^1S_0^{[8]}, {}^1P_1^{[8]}) + c\bar{c}$ are suppressed compared with that of $Z \rightarrow \eta_c({}^1S_0^{[1]}) + c\bar{c}$. For the decay

TABLE VIII. The decay widths (unit:keV) for the decay channels $Z \rightarrow \eta_b(^{2S+1}L_J^{[8]}) + g$ based on two sets of LDMEs, where ‘‘NLO’’ denotes the results up to NLO accuracy. The very large NLO correction in the $^3S_1^{[8]}$ case comes from the contribution of the real correction processes $Z \rightarrow \eta_b(^3S_1^{[8]}) + q\bar{q}$.

Decay channels	Gong <i>et al.</i>	Feng <i>et al.</i>
$\eta_b(^1S_0^{[8]}) + g(\text{LO})$	-6.02×10^{-3}	8.96×10^{-3}
$\eta_b(^1S_0^{[8]}) + g(\text{NLO})$	-1.13×10^{-2}	1.68×10^{-2}
$\eta_b(^3S_1^{[8]}) + g(\text{LO})$	0.346	0.422
$\eta_b(^3S_1^{[8]}) + g(\text{NLO})$	8.27	10.1
$\eta_b(^1P_1^{[8]}) + g(\text{LO})$	-6.23×10^{-2}	-8.65×10^{-2}
$\eta_b(^1P_1^{[8]}) + g(\text{NLO})$	-0.107	-0.149
Total($\eta_b + g$)(LO)	0.278	0.344
Total($\eta_b + g$)(NLO)	8.15	9.97

channels $Z \rightarrow \eta_c(^3S_1^{[8]}) + c\bar{c}(b\bar{b}, q\bar{q})$, the decay widths are dominated by the fragmentation processes of $Z \rightarrow c\bar{c}(b\bar{b}, q\bar{q})$ followed by a quark or an antiquark fragments into the η_c and $Z \rightarrow c\bar{c}g(b\bar{b}g, q\bar{q}g)$ followed by $g \rightarrow \eta_c$. In the fragmentation processes $Z \rightarrow c\bar{c}(b\bar{b}, q\bar{q})$ followed by $c(b, q, \bar{c}, \bar{b}, \bar{q}) \rightarrow \eta_c$, the quark propagator is of order $1/m_{\eta_c}$, and the gluon propagator is $1/m_{\eta_c}^2$. Since the gluon propagator is fixed as $1/m_{\eta_c}^2$ in the whole phase space, the CO channels $Z \rightarrow \eta_c(^3S_1^{[8]}) + c\bar{c}(b\bar{b}, q\bar{q})$ are more important than the CS channel $Z \rightarrow \eta_c(^1S_0^{[1]}) + c\bar{c}$ although the CO channels are suppressed by powers of v_c compared with the CS channel. The decay channels $Z \rightarrow \eta_c(^1S_0^{[8]}, ^3S_1^{[8]}, ^1P_1^{[8]}) + g$ at LO in α_s , have no fragmentation contribution, the quark propagator in these channels is of order $1/m_Z$. Other channels $Z \rightarrow \eta_c(^1S_0^{[8]}, ^1P_1^{[8]}) + b\bar{b}$ and $Z \rightarrow \eta_c(^1S_0^{[1]}) + gg$ also have no fragmentation contribution, thus they are suppressed.³

Due to the fact that the SDCs of the $^3S_1^{[8]}$ channels are greatly enhanced compared to other channels and the $^3S_1^{[8]}$ channels dominate the decay $Z \rightarrow \eta_c + X$, the total decay width of $Z \rightarrow \eta_c + X$ is sensitive to the CO LDME $\langle \mathcal{O}^{\eta_c}(^3S_1^{[8]}) \rangle$. Therefore, the process $Z \rightarrow \eta_c + X$ provides a good platform to determine the value of $\langle \mathcal{O}^{\eta_c}(^3S_1^{[8]}) \rangle$. Moreover, according to HQSS, we have $\langle \mathcal{O}^{\mathcal{J}/\psi}(^1S_0^{[8]}) \rangle = \langle \mathcal{O}^{\eta_c}(^3S_1^{[8]}) \rangle (1 + \mathcal{O}(v_c^2))$. The value of $\langle \mathcal{O}^{\eta_c}(^3S_1^{[8]}) \rangle$ can give a good constraint to the value of $\langle \mathcal{O}^{\mathcal{J}/\psi}(^1S_0^{[8]}) \rangle$.

³Actually, the decay widths for the heavy quarkonium production can be further organized by different powers of m_Q/m_Z under the fragmentation-function approach, more detailed discussions for the power expansion can be found in Refs. [50–55].

TABLE IX. The decay widths (unit:keV) for the decay channels $Z \rightarrow \eta_b(^{2S+1}L_J^{[1,8]}) + b\bar{b}$ based on two sets of LDMEs.

Decay channels	Gong <i>et al.</i>	Feng <i>et al.</i>
$\eta_b(^1S_0^{[1]}) + b\bar{b}$	10.5	10.5
$\eta_b(^1S_0^{[8]}) + b\bar{b}$	-4.65×10^{-4}	6.92×10^{-4}
$\eta_b(^3S_1^{[8]}) + b\bar{b}$	2.49	3.04
$\eta_b(^1P_1^{[8]}) + b\bar{b}$	-2.88×10^{-3}	-3.99×10^{-3}
Total($\eta_b + b\bar{b}$)	13.0	13.5

TABLE X. The decay widths (unit:keV) for the decay channels $Z \rightarrow \eta_b(^{2S+1}L_J^{[8]}) + c\bar{c}$ based on two sets of LDMEs.

Decay channels	Gong <i>et al.</i>	Feng <i>et al.</i>
$\eta_b(^1S_0^{[8]}) + c\bar{c}$	-2.40×10^{-4}	3.58×10^{-4}
$\eta_b(^3S_1^{[8]}) + c\bar{c}$	2.28	2.78
$\eta_b(^1P_1^{[8]}) + c\bar{c}$	-2.18×10^{-3}	-3.02×10^{-3}
Total($\eta_b + c\bar{c}$)	2.28	2.78

Summing the contributions from the considered decay channels, we obtain the decay width for the inclusive process $Z \rightarrow \eta_c + X$ which is given in Table VII.

The contributions to the decay width of $Z \rightarrow \eta_b + X$ from the considered decay channels are given in Tables VIII–XI. The very large NLO correction to the decay channel $Z \rightarrow \eta_b(^3S_1^{[8]}) + g$ comes from the processes $Z \rightarrow \eta_b(^3S_1^{[8]}) + q\bar{q}$ whose decay width is 8.21 keV under the LDME extracted by Gong *et al.* Similar to the η_c case, the dominant contributions come from the decay channels $Z \rightarrow \eta_b(^1S_0^{[1]}, ^3S_1^{[8]}) + b\bar{b}$, $Z \rightarrow \eta_b(^3S_1^{[8]}) + c\bar{c}$, and $Z \rightarrow \eta_b(^3S_1^{[8]}) + q\bar{q}$ due to the fragmentation mechanism in these channels.

TABLE XI. The decay width (unit:keV) for the decay channel $Z \rightarrow \eta_b(^1S_0^{[1]}) + gg$ based on two sets of LDMEs.

Decay channels	Gong <i>et al.</i>	Feng <i>et al.</i>
$\eta_b(^1S_0^{[1]}) + gg$	2.10	2.10

TABLE XII. The decay width (unit:keV) for $Z \rightarrow \eta_b + X$ based on two sets of LDMEs.

	Gong <i>et al.</i>	Feng <i>et al.</i>
$\eta_b + X$	25.5	28.4

Different from the η_c case, among these dominant decay channels, the CS channel $Z \rightarrow \eta_b(1S_0^{[1]}) + b\bar{b}$ is the most important channel. There are two reasons: one is that m_Z/m_{η_b} is smaller than m_Z/m_{η_c} , which leads to the enhancement in the SDCs of the ${}^3S_1^{[8]}$ channels is weakened for the η_b case. The other is that the CO LDME $\langle \mathcal{O}^{\eta_c}({}^3S_1^{[8]}) \rangle$ is more suppressed compared with the CS LDME $\langle \mathcal{O}^{\eta_c}(1S_0^{[1]}) \rangle$ in the η_b case. However, for the ${}^3S_1^{[8]}$ channels, since the final open quark pair can be several flavors, the sum of these ${}^3S_1^{[8]}$ channels dominate the decay $Z \rightarrow \eta_b + X$. Therefore, the decay $Z \rightarrow \eta_b + X$ can be used to determine the value of $\langle \mathcal{O}^{\eta_b}({}^3S_1^{[8]}) \rangle$, and give a good constraint to the value of $\langle \mathcal{O}^{\Upsilon}(1S_0^{[8]}) \rangle$.

Summing the contributions from the considered decay channels, we obtain the decay width for the inclusive process $Z \rightarrow \eta_b + X$ which is presented in Table XII.

B. Differential decay widths

In this subsection, we present the differential decay widths $d\Gamma/dz$ for $Z \rightarrow \eta_Q + X$, where the energy fraction is defined as $z \equiv 2p_{\eta_Q} \cdot p_Z/p_Z^2$. Since the dominant contributions to the decay process $Z \rightarrow \eta_Q + X$ come from the $1S_0^{[1]}$ and ${}^3S_1^{[8]}$ channels and the contributions from other channels are greatly suppressed, we only consider the $1S_0^{[1]}$ and ${}^3S_1^{[8]}$ channels in this subsection.

The differential decay widths $d\Gamma/dz$ for $Z \rightarrow \eta_c + X$ based on the three sets of LDMEs are given in Fig. 10. From the figure, we can see that the ${}^3S_1^{[8]}$ channels dominate the decay $Z \rightarrow \eta_c + X$, which was also shown in the last subsection by the integrated decay widths. The distributions of the CS channel and the CO channels have different shapes. The curve of the CS channel has a peak at a moderate z value, while the curves of the CO channels have a peak at a small z value. This feature can be used to determine the CS LDME $\langle \mathcal{O}^{\eta_c}(1S_0^{[1]}) \rangle$ and the CO LDME $\langle \mathcal{O}^{\eta_c}({}^3S_1^{[8]}) \rangle$ more precisely.

The differential decay widths for $Z \rightarrow \eta_b + X$ based on the two sets of the LDMEs are given in Fig. 11. Here, the differential decay width of the channel $\eta_b(1S_0^{[1]}) + gg$ is also given. Similar to the η_c case, the curves of the CS channels have a peak at a moderate z value while the curves of the CO channels have a peak at a small z value. However, since the CS contribution is comparable with the CO contribution in the η_b case, the shape of the inclusive process $Z \rightarrow \eta_b + X$ is significantly different from that of $Z \rightarrow \eta_c + X$.

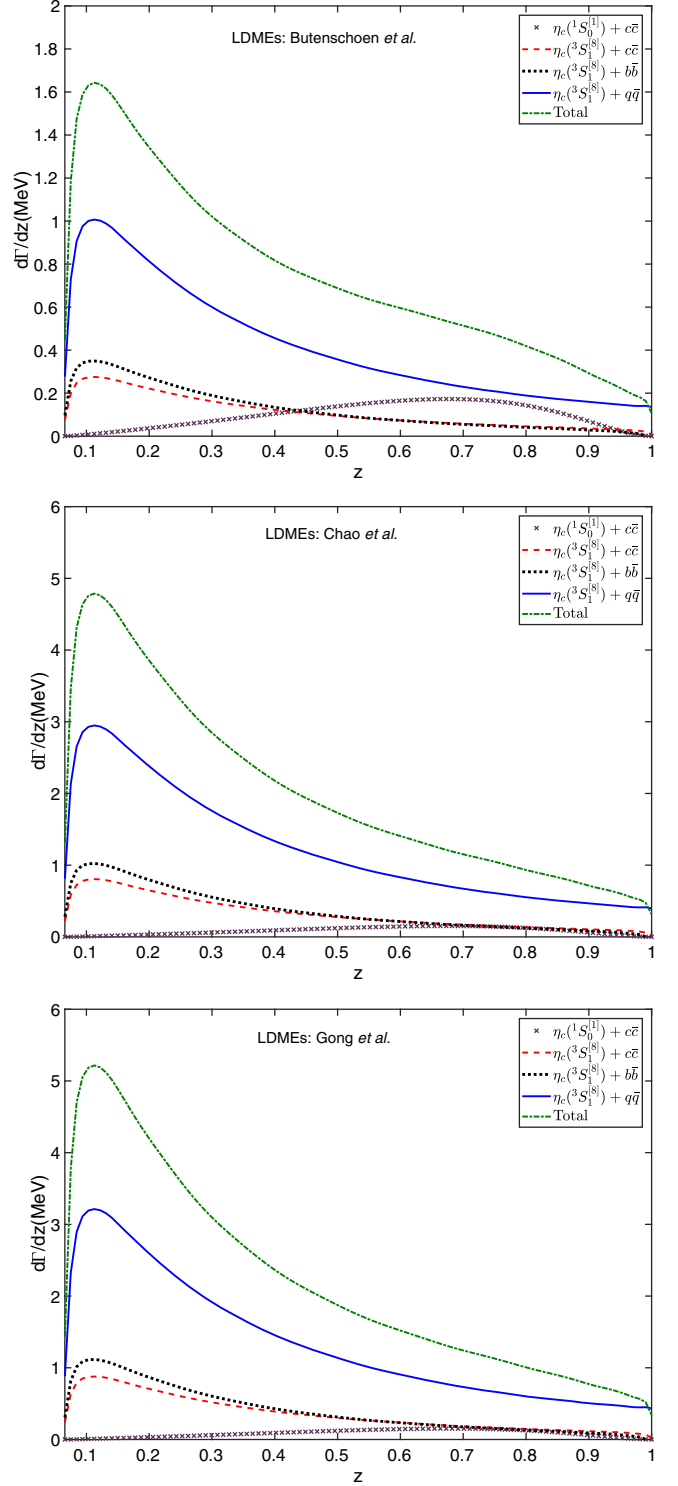


FIG. 10. The differential decay widths $d\Gamma/dz$ for $Z \rightarrow \eta_c + X$, where $\mu_R = 2m_c$. The top one shows the distributions based on the LDMEs of Butenschoen *et al.* [4], the middle one shows the distributions based the LDMEs of Chao *et al.* [5], and the bottom one shows the distributions based the LDMEs of Gong *et al.* [6].

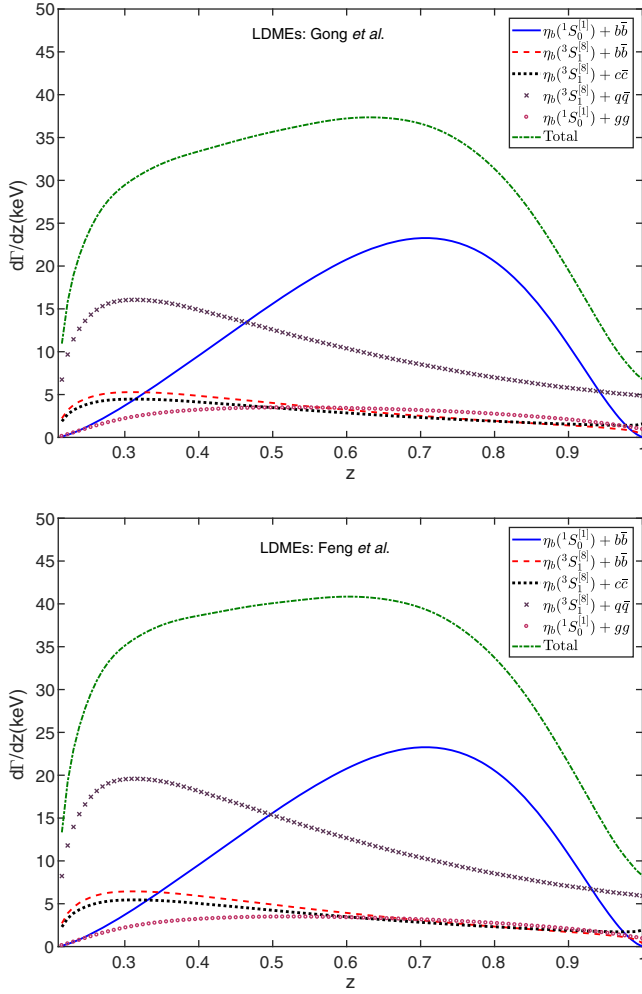


FIG. 11. The differential decay widths $d\Gamma/dz$ for $Z \rightarrow \eta_c + X$, where $\mu_R = 2m_b$. The top one shows the distributions based on the LDMEs of Gong *et al.* [48], and the bottom one shows the distributions based the LDMEs of Feng *et al.* [49].

IV. DISCUSSION AND CONCLUSION

In the present paper, we have studied the inclusive production of η_Q ($Q = c$ or b) through Z boson decays. The CS ($1S_0^{[1]}$) and the CO ($1S_0^{[8]}$, $3S_1^{[8]}$, and $1P_1^{[8]}$) Fock states are considered. The integrated and differential decay widths for the related channels are computed, and the results show that the decay width of $Z \rightarrow \eta_Q + X$ is dominated by the CO $3S_1^{[8]}$ production. It means that the decay width of $Z \rightarrow \eta_Q + X$ is sensitive to the value of the LDME $\langle \mathcal{O}^{\eta_Q}(3S_1^{[8]}) \rangle$. Hence, the two processes $Z \rightarrow \eta_c + X$ and $Z \rightarrow \eta_b + X$ can be used to determine the values of $\langle \mathcal{O}^{\eta_c}(3S_1^{[8]}) \rangle$ and $\langle \mathcal{O}^{\eta_b}(3S_1^{[8]}) \rangle$. Moreover, via HQSS, the measured value of $\langle \mathcal{O}^{\eta_Q}(3S_1^{[8]}) \rangle$ from the process $Z \rightarrow \eta_Q + X$ can also give a certain constraint on the value of $\langle \mathcal{O}^{J/\psi(\Upsilon)}(1S_0^{[8]}) \rangle$. Note that this conclusion depends partly on the exact values of

LDMEs, and it is applicable only if the LDMEs are at the same order of magnitude of the ones quoted in this paper.

The differential distributions $d\Gamma/dz$ are shown in figures. The distributions of the CS and the CO components are very different. The distributions of the CS component have a peak at a moderate z value, while the distributions of the CO components have a peak at a small z value. Thus, the CS LDME $\langle \mathcal{O}^{\eta_Q}(1S_0^{[1]}) \rangle$ and the CO LDME $\langle \mathcal{O}^{\eta_Q}(3S_1^{[8]}) \rangle$ can be determined more precisely through measuring the energy distribution of the process $Z \rightarrow \eta_Q + X$.

In a hadronic collider such as the LHC, the production of the heavy quarkonium η_Q is dominated by hadronic production, so it is difficult to pick up the production events via Z decays. Thus the calculations on the production via Z boson decays here may be really useful as reference mainly for the production in a super Z factory. The total cross section for the η_Q production via the electron and positron annihilation at the Z pole, $e^+e^- \rightarrow Z \rightarrow \eta_Q + X^4$ can be derived from the decay width $\Gamma_{Z \rightarrow \eta_Q + X}$ through the formula derived in the Appendix A1 of Ref. [56], i.e.,

$$\sigma_{e^+e^- \rightarrow \eta_Q + X} = \frac{e^2(1 - 4\sin^2\theta_W + 8\sin^4\theta_W)}{8\sin^2\theta_W \cos^2\theta_W m_Z \Gamma_Z^2} \Gamma_{Z \rightarrow \eta_Q + X}. \quad (40)$$

Then we obtain

$$\sigma_{e^+e^- \rightarrow \eta_c + X} = 45.0 \text{ pb}, \quad (41)$$

$$\sigma_{e^+e^- \rightarrow \eta_b + X} = 0.608 \text{ pb}, \quad (42)$$

where the input values for the LDMEs have been taken as those extracted by Chao *et al.* [5] and Gong *et al.* [48], which have been presented in Tables I and II. If the luminosity of a Z factory can be up to $10^{35} \text{ cm}^{-2} \text{ s}^{-1}$ [22], then there are about $4.5 \times 10^7 \eta_c$ and $6.1 \times 10^5 \eta_b$ to be produced per operation year. Therefore, at a high luminosity Z factory with highly rejecting backgrounds, those two production processes can be studied thoroughly.

ACKNOWLEDGMENTS

This work was supported in part by the Natural Science Foundation of China under Grants No. 11625520, No. 12005028, No. 11675239, No. 11745006, No. 11821505, No. 12075301, and No. 12047564, by the China Postdoctoral Science Foundation under Grant No. 2021M693743, by the Fundamental Research Funds for the Central Universities under Grant No. 2020CQJQY-Z003, and by the Chongqing Graduate Research and Innovation Foundation under Grant No. ydstd1912.

⁴The γ -exchange contribution is negligibly small at the Z pole, which can be safely neglected.

- [1] G. T. Bodwin, E. Braaten, and G. P. Lepage, Rigorous QCD analysis of inclusive annihilation and production of heavy quarkonium, *Phys. Rev. D* **51**, 1125 (1995); **55**, 5853(E) (1997).
- [2] N. Brambilla *et al.*, Heavy quarkonium: Progress, puzzles, and opportunities, *Eur. Phys. J. C* **71**, 1534 (2011) and references therein.
- [3] N. Brambilla *et al.*, Heavy Quarkonium Physics, Report No. CERN-2005-005 2005, [arXiv:hep-ph/0412158](https://arxiv.org/abs/hep-ph/0412158).
- [4] M. Butenschoen and B. A. Kniehl, World data of J/ψ production consolidate NRQCD factorization at NLO, *Phys. Rev. D* **84**, 051501 (2011).
- [5] K. T. Chao, Y. Q. Ma, H. S. Shao, K. Wang, and Y. J. Zhang, J/ψ Polarization at Hadron Colliders in Nonrelativistic QCD, *Phys. Rev. Lett.* **108**, 242004 (2012).
- [6] B. Gong, L. P. Wan, J. X. Wang, and H. F. Zhang, Polarization for Prompt J/ψ and $\psi(2s)$ Production at the Tevatron and LHC, *Phys. Rev. Lett.* **110**, 042002 (2013).
- [7] N. Brambilla, S. Eidelman *et al.*, QCD and strongly coupled gauge theories: challenges and perspectives, *Eur. Phys. J. C* **74**, 2981 (2014).
- [8] P. A. Zyla *et al.* (Particle Data Group), Review of particle physics, *Prog. Theor. Exp. Phys.* **2020**, 083C01 (2020).
- [9] S. Barsuk, J. He, E. Kou, and B. Viaud, Investigating charmonium production at LHC with the $p\bar{p}$ final state, *Phys. Rev. D* **86**, 034011 (2012).
- [10] R. Aaij *et al.* (LHCb Collaboration), Measurement of the $\eta_c(1S)$ production cross-section in proton-proton collisions via the decay $\eta_c(1S) \rightarrow p\bar{p}$, *Eur. Phys. J. C* **75**, 311 (2015).
- [11] R. Aaij *et al.* (LHCb Collaboration), Measurement of the $\eta_c(1S)$ production cross-section in pp collisions at $\sqrt{s} = 13$ TeV, *Eur. Phys. J. C* **80**, 191 (2020).
- [12] M. Butenschoen, Z. G. He, and B. A. Kniehl, η_c Production at the LHC Challenges Nonrelativistic-QCD Factorization, *Phys. Rev. Lett.* **114**, 092004 (2015).
- [13] H. Han, Y. Q. Ma, C. Meng, H. S. Shao, and K. T. Chao, η_c Production at LHC and Indications on the Understanding of J/ψ Production, *Phys. Rev. Lett.* **114**, 092005 (2015).
- [14] H. F. Zhang, Z. Sun, W. L. Sang, and R. Li, Impact of η_c Hadroproduction Data on Charmonium Production and Polarization Within NRQCD Framework, *Phys. Rev. Lett.* **114**, 092006 (2015).
- [15] V. P. Goncalves and B. D. Moreira, η_c production in photon-induced interactions at the LHC, *Phys. Rev. D* **97**, 094009 (2018).
- [16] Y. Feng, J. He, J. P. Lansberg, H. S. Shao, A. Usachov, and H. F. Zhang, Phenomenological NLO analysis of η_c production at the LHC in the collider and fixed-target modes, *Nucl. Phys.* **B945**, 114662 (2019).
- [17] S. P. Baranov and A. V. Lipatov, Prompt η_c meson production at the LHC in the NRQCD with k_T -factorization, *Eur. Phys. J. C* **79**, 621 (2019).
- [18] I. Babiarez, R. Pasechnik, W. Schäfer, and A. Szczurek, Prompt hadroproduction of $\eta_c(1S, 2S)$ in the k_T -factorization approach, *J. High Energy Phys.* **02** (2020) 037.
- [19] Tichouk, H. Sun, and X. Luo, Hard diffractive $\eta_{c,b}$ hadroproduction at the LHC, *Phys. Rev. D* **101**, 054035 (2020).
- [20] Tichouk, H. Sun, and X. Luo, Inclusive diffractive η_c production in pp , pA and AA modes at the LHC, *Phys. Rev. D* **101**, 094006 (2020).
- [21] A. Law, Measurement of the inclusive cross sections for production of w and z bosons decaying to electronic and muonic final states in 13 TeV center-of-mass energy proton-proton collisions with the ATLAS detector, Ph.D. thesis.
- [22] J. P. Ma and Z. X. Zhang, (The Super Z-Factory Group), Preface, *Sci. China Phys., Mech. Astron.* **53**, 1947 (2010).
- [23] B. Guberina, J. H. Kuhn, R. D. Peccei, and R. Ruckl, Rare decays of the Z^0 , *Nucl. Phys.* **B174**, 317 (1980).
- [24] W. Y. Keung, Off resonance production of heavy vector quarkonium states in e^+e^- annihilation, *Phys. Rev. D* **23**, 2072 (1981).
- [25] K. J. Abraham, Bottomium production at LEP, *Z. Phys. C* **44**, 467 (1989).
- [26] V. D. Barger, K. M. Cheung, and W. Y. Keung, Z-boson decays to heavy quarkonium, *Phys. Rev. D* **41**, 1541 (1990).
- [27] K. Hagiwara, A. D. Martin, and W. J. Stirling, J/ψ production from gluon jets at LEP, *Phys. Lett. B* **267**, 527 (1991).
- [28] E. Braaten, K. m. Cheung, and T. C. Yuan, Z^0 decay into charmonium via charm quark fragmentation, *Phys. Rev. D* **48**, 4230 (1993).
- [29] S. Fleming, Electromagnetic production of quarkonium in Z^0 decay, *Phys. Rev. D* **48**, R1914 (1993).
- [30] Q. L. Liao, Y. Yu, Y. Deng, G. Y. Xie, and G. C. Wang, Excited heavy quarkonium production via Z^0 decays at a high luminosity collider, *Phys. Rev. D* **91**, 114030 (2015).
- [31] P. Ernstrom, L. Lonnblad, and M. Vanttinen, Evolution effects in Z^0 fragmentation into charmonium, *Z. Phys. C* **76**, 515 (1997).
- [32] G. A. Schuler, Quarkonium production: Velocity scaling rules and long distance matrix elements, *Int. J. Mod. Phys. A* **12**, 3951 (1997).
- [33] K. M. Cheung, W. Y. Keung, and T. C. Yuan, Color Octet Quarkonium Production at the Z Pole, *Phys. Rev. Lett.* **76**, 877 (1996).
- [34] P. L. Cho, Prompt upsilon and psi production at LEP, *Phys. Lett. B* **368**, 171 (1996).
- [35] R. Li and J. X. Wang, Next-to-leading-order QCD correction to inclusive $J/\Psi(\Upsilon)$ production in Z^0 decay, *Phys. Rev. D* **82**, 054006 (2010).
- [36] X. C. Zheng, C. H. Chang, and X. G. Wu, NLO fragmentation functions of heavy quarks into heavy quarkonia, *Phys. Rev. D* **100**, 014005 (2019).
- [37] J. G. Korner, D. Kreimer, and K. Schilcher, A Practicable $\gamma(5)$ scheme in dimensional regularization, *Z. Phys. C* **54**, 503 (1992).
- [38] M. Beneke and V. A. Smirnov, Asymptotic expansion of Feynman integrals near threshold, *Nucl. Phys.* **B522**, 321 (1998).
- [39] B. W. Harris and J. F. Owens, The Two cutoff phase space slicing method, *Phys. Rev. D* **65**, 094032 (2002).
- [40] T. Hahn, Generating Feynman diagrams and amplitudes with FeynArts 3, *Comput. Phys. Commun.* **140**, 418 (2001).
- [41] R. Mertig, M. Bohm, and A. Denner, FeynCalc—Computer-algebraic calculation of Feynman amplitudes, *Comput. Phys. Commun.* **64**, 345 (1991).
- [42] V. Shtabovenko, R. Mertig, and F. Orellana, New developments in FeynCalc 9.0, *Comput. Phys. Commun.* **207**, 432 (2016).

- [43] F. Feng, \$Apart: A generalized Mathematica apart function, *Comput. Phys. Commun.* **183**, 2158 (2012).
- [44] A. V. Smirnov, Algorithm FIRE—Feynman Integral REduction, *J. High Energy Phys.* **10** (2008) 107.
- [45] T. Hahn and M. Perez-Victoria, Automated one loop calculations in four-dimensions and D-dimensions, *Comput. Phys. Commun.* **118**, 153 (1999).
- [46] G. P. Lepage, A new algorithm for adaptive multidimensional integration, *J. Comput. Phys.* **27**, 192 (1978).
- [47] C. Patrignani *et al.* (Particle Data Group), Review of particle physics, *Chin. Phys. C* **40**, 100001(2016).
- [48] B. Gong, L. P. Wan, J. X. Wang, and H. F. Zhang, Complete Next-to-Leading-Order Study on the Yield and Polarization of $\Upsilon(1S, 2S, 3S)$ at the Tevatron and LHC, *Phys. Rev. Lett.* **112**, 032001 (2014).
- [49] Y. Feng, B. Gong, L. P. Wan, and J. X. Wang, An updated study of Υ production and polarization at the Tevatron and LHC, *Chin. Phys. C* **39**, 123102 (2015).
- [50] C. H. Chang, Y. Q. Chen, G. P. Han, and H. T. Jiang, On hadronic production of the B(c) meson, *Phys. Lett. B* **364**, 78 (1995).
- [51] Z. B. Kang, J. W. Qiu, and G. Sterman, Factorization and quarkonium production, *Nucl. Phys. B, Proc. Suppl.* **214**, 39 (2011).
- [52] Z. B. Kang, J. W. Qiu, and G. Sterman, Heavy Quarkonium Production and Polarization, *Phys. Rev. Lett.* **108**, 102002 (2012).
- [53] Z. B. Kang, Y. Q. Ma, J. W. Qiu, and G. Sterman, Heavy quarkonium production at collider energies: Factorization and evolution, *Phys. Rev. D* **90**, 034006 (2014).
- [54] K. Lee and G. Sterman, Power expansion for heavy quarkonium production at next-to-leading order in e^+e^- annihilation, *J. High Energy Phys.* **09** (2020) 046.
- [55] S. Fleming, A. K. Leibovich, T. Mehen, and I. Z. Rothstein, The systematics of quarkonium production at the LHC and double parton fragmentation, *Phys. Rev. D* **86**, 094012 (2012).
- [56] X. C. Zheng, C. H. Chang, T. F. Feng, and Z. Pan, NLO QCD corrections to $B_c(B^*_c)$ production around the Z pole at an e^+e^- collider, *Sci. China Phys. Mech. Astron.* **61**, 031012 (2018).